

Vibronic effect on resonant inelastic x-ray scattering in cubic iridium hexahalides

Naoya Iwahara^{1,*} and Wataru Furukawa²

¹*Graduate School of Engineering, Chiba University,*

1-33 Yayoi-cho, Inage-ku, Chiba-shi, Chiba 263-8522, Japan

²*Department of Materials Science, Faculty of Engineering, Chiba University,*

1-33 Yayoi-cho, Inage-ku, Chiba-shi, Chiba 263-8522, Japan

(Dated: May 23, 2023)

In resonant inelastic x-ray scattering (RIXS) spectra of K_2IrCl_6 , the peak for the $j = 3/2$ multiplet states shows a splitting that resembles non-cubic crystal-field effect although the compound is cubic down to 0.3 K. Here we theoretically describe the RIXS spectra concomitantly treating the spin-orbit and vibronic interactions. We found that the dynamic Jahn-Teller effect in the $j = 3/2$ multiplet states gives rise to the splitting of the RIXS spectra and the broadening of the spectra in raising the temperature. The validity of the interaction parameters for the simulations is supported by our *ab initio* calculations. Our results suggest that, in cubic iridium compounds, the dynamic Jahn-Teller effect induces the splitting of RIXS spectra without lowering the symmetry.

I. INTRODUCTION

Strong spin-orbit coupling gives rise to rich quantum phenomena in $4d/5d$ transition metal compounds [1–3]. One of the most investigated phenomena is the Kitaev spin liquid phase in Mott-insulating honeycomb compounds [4]. The candidate honeycomb materials consist of edge-sharing octahedra containing heavy d^5 ions. The spin-orbit coupling of the d^5 ion in the octahedral environment makes the local quantum states spin-orbit entangled $j = 1/2$ type and the exchange interaction between the d^5 sites bond-dependent (Kitaev-type anisotropy). The Kitaev exchange interaction appears in other lattices such as triangular and face centered cubic (fcc) lattices [4], which could induce various magnetic phases [5, 6].

Motivated by the theoretical predictions, much experimental effort has been made to search Kitaev and related systems, while realizing pure $j = 1/2$ states in materials is far from trivial. Contrary to the assumption of a perfect octahedral environment in theories, candidate materials exhibit symmetry lowering, resulting in the hybridization of the $j = 1/2$ and the excited $j = 3/2$ states.

Recently, K_2IrCl_6 was reported as the first iridium compound with pure $j = 1/2$ states on metal sites [7]. The neutron powder diffraction data show that the compound is cubic down to 0.3 K [8]. The g -tensor measured by electron paramagnetic resonance is consistent with the g for $j = 1/2$ in an octahedral environment, suggesting no symmetry lowering [9].

Nevertheless, spectroscopic data look controversial to the cubic structure of K_2IrCl_6 . Within the octahedral environment, the excited states of a single Ir site are four-fold degenerate $j = 3/2$ multiplet. In contrast, the resonance inelastic x-ray scattering (RIXS) measurement of the $j = 3/2$ states shows a splitting of ≈ 50 meV down to low temperature (10 K) [8]. The RIXS spectra of cu-

bic K_2IrBr_6 (in high-temperature phase) and Cs_2IrCl_6 resemble those of K_2IrCl_6 too [8, 10, 11]. The Raman scattering spectra of K_2IrCl_6 also show a similar splitting in the same range of energy [12]. As the origin of the splitting, non-cubic deformation of each octahedron and crystal-field splitting by rotational modes of the octahedra were discussed. In both cases, the symmetry of the system becomes lower than the cubic one. Moreover, the latter leads to the splitting of only a few meV according to the previous experiments and calculations [10].

We recently proved *ab initio* that the vibronic excitations induce the splittings of peaks in the RIXS spectra of a similar compound, K_2RuCl_6 [13, 14]. In this compound, the dynamic Jahn-Teller (JT) effect develops in the excited spin-orbit multiplet states and determines the shape and temperature evolution of the RIXS spectra. The dynamic JT effect is characterized by the superpositions of many electron-lattice configurations with JT-deformed structures, and hence, structural anisotropy does not appear in K_2RuCl_6 . Since the vibronic coupling tends to be stronger in $5d$ systems than in $4d$ systems [15], the dynamic JT effect would give nonnegligible changes in the RIXS spectra of the Ir compounds.

In this work, we examine the presence of the dynamic JT effect and reveal its impact on the RIXS spectra of the Ir^{4+} compounds. We calculate the vibronic states of the dynamic JT model and, based on them, the RIXS spectra. We confirm the validity of the derived interaction parameters by a series of post Hartree-Fock calculations.

II. VIBRONIC MODEL FOR $5d^5$ ION

Here we explain the theoretical framework for the quantum states and the RIXS spectra of a single Ir site in the cubic K_2IrX_6 ($X = \text{Cl}, \text{Br}$). We discuss only the phenomena in a single Ir octahedron because the energy scale of the intersite exchange interaction (about 1 meV) [7, 9, 10] is several tens times smaller than the splitting (about 35–60 meV) in the RIXS spectra [8, 10].

The quantum states of each $5d^5$ site are determined

* naoya.iwahara@gmail.com

by the interplay of the ligand field, spin-orbit, and vibronic interactions. We consider the interactions in the order because their energy scales decrease from several eV by about one order of magnitude. The octahedral ligand field splits the $5d$ orbitals into e_g doublet and t_{2g} triplet. The t_{2g} orbitals are lower in energy and have five electrons (one hole). Hereafter, we use the hole picture. Within the t_{2g} orbitals, the spin-orbit coupling is unquenched [16]:

$$\hat{H}_{\text{SO}} = -\lambda \tilde{\mathbf{l}} \cdot \hat{\mathbf{s}}, \quad (1)$$

where $\tilde{\mathbf{l}}$ is the effective $\tilde{l} = 1$ orbital operator, $\hat{\mathbf{s}}$ is the spin operator, and $\lambda (> 0)$ is the spin-orbit coupling parameter. The t_{2g} hole couples to the JT active E_g vibrations too: the JT model including the harmonic oscillator Hamiltonian for the E_g modes is [17]

$$\begin{aligned} \hat{H}_{\text{JT}} = & \sum_{\gamma=u,v} \frac{\hbar\omega}{2} (\hat{p}_\gamma^2 + \hat{q}_\gamma^2) - \hbar\omega g \left[\left(-\frac{1}{2}\hat{q}_u + \frac{\sqrt{3}}{2}\hat{q}_v \right) \hat{P}_{yz} \right. \\ & \left. + \left(-\frac{1}{2}\hat{q}_u - \frac{\sqrt{3}}{2}\hat{q}_v \right) \hat{P}_{zx} + \hat{q}_u \hat{P}_{xy} \right]. \end{aligned} \quad (2)$$

Here \hat{q}_γ are the dimensionless normal coordinates for the E_g modes ($\gamma = u, v$, where u and v transform as z^2 and $x^2 - y^2$, respectively), \hat{p}_γ the conjugate momenta of \hat{q}_γ , ω the frequency of the E_g modes, g the dimensionless vibronic coupling parameter, and \hat{P}_γ ($\gamma = yz, zx, xy$) is the projection operator into the $t_{2g}\gamma$ orbital. We ignore the vibronic coupling to the T_{2g} modes because it is much weaker than that to the E_g modes.

The spin-orbit interaction splits the t_{2g}^1 hole configurations into effective $j = 1/2$ and $j = 3/2$ multiplet states. These states belong to the eigen energies of \hat{H}_{SO} , $-\frac{\lambda}{2}$ and λ , respectively. Using the spin-orbit multiplet states, the vibronic coupling part of \hat{H}_{JT} becomes

$$\frac{\hbar\omega g}{2} \begin{pmatrix} 0 & 0 & 0 & \sqrt{2}\hat{q}_v & 0 & -\sqrt{2}\hat{q}_u \\ 0 & 0 & \sqrt{2}\hat{q}_u & 0 & -\sqrt{2}\hat{q}_v & 0 \\ 0 & \sqrt{2}\hat{q}_u & -\hat{q}_u & 0 & -\hat{q}_v & 0 \\ \sqrt{2}\hat{q}_v & 0 & 0 & \hat{q}_u & 0 & -\hat{q}_v \\ 0 & -\sqrt{2}\hat{q}_v & -\hat{q}_v & 0 & \hat{q}_u & 0 \\ -\sqrt{2}\hat{q}_u & 0 & 0 & -\hat{q}_v & 0 & -\hat{q}_u \end{pmatrix}. \quad (3)$$

The basis of the matrix is in the order of $j = \frac{1}{2}$ ($m_j = -\frac{1}{2}, \frac{1}{2}$) and $j = \frac{3}{2}$ ($m_j = -\frac{3}{2}, -\frac{1}{2}, \frac{1}{2}, \frac{3}{2}$). Eq. (3) indicates the presence of the JT effect in the $j = 3/2$ multiplet states and the pseudo JT effect between the $j = 1/2$ and $j = 3/2$ spin-orbit multiplets.

The energy eigenstates of $5d^5$ sites take the form of spin-orbit and lattice entanglement. Since the vibronic interaction, Eq. (3), hybridizes the spin-orbit multiplet states via the quantized normal coordinates, the energy eigenstates (vibronic states) of $\hat{H}_{\text{SO}} + \hat{H}_{\text{JT}}$ are

$$|\psi_\nu\rangle = \sum_{jm_j} |jm_j\rangle \otimes |\chi_{jm_j;\nu}\rangle, \quad (4)$$

where $|\chi_{jm_j;\nu}\rangle$ include the information of the lattice degrees of freedom. The vibronic states reduce to the direct products of the spin-orbit multiplet and vibrational states in the limit of $g \rightarrow 0$.

Now, we turn to the Ir L_3 RIXS spectra of the vibronic system. The L_3 RIXS is a photon-in photon-out process involving an electron transitions from the $2p_{3/2}$ states to the $5d$ orbitals, and then, from the $5d$ orbitals to the $2p_{3/2}$ within an Ir ion. Assuming that the initial and final states of the system are of vibronic type, Eq. (4), the cross-section for the L_3 RIXS process in a single Ir center is [14]

$$\begin{aligned} \frac{d^2\sigma}{d\Omega dk'} \propto & \sum_{\nu} \rho_{\nu} \frac{k'}{k} \left| \sum_{\alpha'\alpha} \epsilon_{\mathbf{k}'\lambda',\alpha'} \epsilon_{\mathbf{k}\lambda,\alpha} \langle \nu' | \hat{d}_{\alpha'} \hat{P}_{\text{eh}} \hat{d}_{\alpha} | \nu \rangle \right|^2 \\ & \times \delta(E_{\nu} + \hbar\omega - E_{\nu'} - \hbar\omega'), \end{aligned} \quad (5)$$

by using the Kramers-Heisenberg formula [18, 19] and the dipole and fast collision approximations [20, 21]. In Eq. (5), ν (ν') indicate the initial (final) vibronic states, ρ_{ν} the canonical distribution for the Ir center, \hat{d}_{α} the α ($= x, y, z$) component of the electric dipole operator, \hat{P}_{eh} the projection operator into the electron-hole states with $(2p_{3/2})^3(5d)^6$ electron configurations, and $\hbar\omega_i$ ($\hbar\omega_f$) and $\epsilon_{\mathbf{k}\lambda}$ ($\epsilon_{\mathbf{k}'\lambda'}$) are, respectively, the energy and the polarization of the incident (scattered) photon.

III. COMPUTATIONAL METHODS

For the derivation of the vibronic states, Eq. (4), we performed a numerical diagonalization of the model Hamiltonian [see e.g. Refs. [14, 15, 22]]. We calculated the Hamiltonian matrix of the JT model, we used the direct products of the $|j, m_j\rangle$ ($j = \frac{1}{2}, \frac{3}{2}$) and the eigenstates of the harmonic oscillator part of \hat{H}_{JT} , $|n_u, n_v\rangle$ ($n_u, n_v = 0, 1, 2, \dots$), as the basis. We expanded the lattice parts of the vibronic states, Eq. (4), as

$$|\chi_{jm_j;\nu}\rangle = \sum_{n_u, n_v} |n_u, n_v\rangle C_{jm_j, n_u, n_v; \nu}. \quad (6)$$

We truncated our basis so that $0 \leq n_u + n_v \leq 15$.

The dynamic JT Hamiltonian contains interaction parameters, λ , ω , and g . We took λ from the RIXS data and ω from the Raman scattering data and treated g as a variable. We determined g so that we can reproduce the experimental RIXS spectra.

To check the validity of the chosen parameters, we also derived all the interaction parameters by a series of post Hartree-Fock calculations as in Refs. [14, 15, 22]. We made clusters of K_2IrCl_6 and K_2IrBr_6 using the neutron diffraction data at 0.3 K for the former and 200 K for the latter, respectively [8]. Each cluster consists of three groups of atoms. The first group corresponds to K_8IrX_6 ($X = \text{Cl}, \text{Br}$) cluster, which we treated *ab initio* with atomic-natural-orbital relativistic-correlation consistent-valence quadruple- ζ polarization basis set. The second

group contains the nearest 12 octahedra and the neighboring 48 K atoms, which are replaced by *ab initio* embedded potential [23]. The third part consists of point charges. The total charge of the entire cluster is neutral. We calculated $^2T_{2g}$ states of the clusters with the complete active space self-consistent field (CASSCF) method [24] followed by a correction within the extended multistate complete active space second-order perturbation theory (XMS-CASPT2) [25, 26], and then, the spin-orbit j multiplet states with spin-orbit restricted active space state interaction (SO-RASSI) method [24] implemented in *OpenMolcas* [27, 28]. In these calculations, we set three $5d\ t_{2g}$ orbitals with one hole as the active space. We determined λ by using the SO-RASSI energy gap.

For the calculations of the vibronic coupling parameters and the frequencies, we fit the $^2T_{2g}$ adiabatic potential energy surfaces with respect to the JT deformation to the JT model, Eq. (2) [See Refs. [14, 15, 22]]. The relation between the JT-deformed Cartesian coordinates and normal coordinates is $\mathbf{R}_A = \mathbf{R}_A^{(0)} + Q_u (\mathbf{e}_{Eu})_A / \sqrt{M}$, where \mathbf{R}_A are the Cartesian coordinates of ligand atom A , $\mathbf{R}^{(0)}$ indicates the experimental octahedral configurations, \mathbf{e}_{Eu} is the JT-active Eu polarization vectors of the neighboring six Cl's or Br's, Q_u the mass-weighted normal coordinates ($Q_u = \sqrt{\hbar/\omega q_u}$), and M the mass of ligand atoms.

IV. RESULTS AND DISCUSSIONS

A. Vibronic spectra

We calculated the vibronic levels of the dynamic JT model for a single Ir^{4+} site. For the calculations, we used the interaction parameters from the experiments of K_2IrCl_6 : $\lambda = 0.436$ eV [8] and $\omega = 37.1$ meV [12]. We reduced the reported λ by 0.04 eV for a better agreement between the theoretical and experimental RIXS spectra (Sec. IV B).

The vibronic spectra around the excited spin-orbit $j = 3/2$ multiplet level show nontrivial distribution of the energy levels. Figure 1(a) indicates the energy spectra with respect to g : the distribution of the vibronic levels for $|g| > 0$ differs from that without the JT effect ($g = 0$). Each level is either two-fold (the points) or four-fold (the open circles) degenerate.

We also calculated the vibronic states of K_2IrBr_6 . We used $\lambda = 0.395$ eV [10] and $\omega = 24.7$ meV. We reduced λ from the experimental value by 0.05 eV. We estimated ω by assuming that the elastic couplings K for the E_g modes are common for K_2IrCl_6 and K_2IrBr_6 and using $\omega \propto \sqrt{K/M}$. The pattern of the calculated vibronic states of K_2IrBr_6 resembles that of K_2IrCl_6 .

B. Vibronic peaks in RIXS spectra

With the derived vibronic states, we calculated the RIXS spectra around the $j = 3/2$ multiplet level at 10 K using Eq. (5). We set the incident and scattered photons following the experimental condition [8]. We convoluted the cross-section with the Lorentzian function with width $\Gamma = 50$ meV. Varying g , the shape of the RIXS spectrum changes [Fig. 1(b)]. When $g = 0$, the RIXS spectrum has only one peak. As g increases, the peak splits into a few originating from the transitions between the ground spin-orbit $j = 1/2$ states and several excited vibronic states (see the blue vertical lines).

The calculated RIXS spectrum with $g = 1.2$ agrees well with the experimental one from Ref. [8] [Fig. 1(c)]. The calculated spectrum has two strong peaks at about 0.645 eV and 0.690 eV corresponding to the transitions between the ground $j = 1/2$ multiplet and the four-fold degenerate vibronic states [The lowest two four-fold degenerate levels in Fig. 1(a)]. The gap between the peaks is about 45 meV, which is close to the experimental estimation of 48 meV.

Raising the temperature from 10 K to 300 K, the shape of the RIXS spectrum changes. The height of the main peak at 0.645 eV decreases, and the width increases as the temperature rises. These temperature dependencies agree with those of the experimental data. The temperature evolution of the spectra occurs due to the transitions from the thermally populated states with vibrational excitations to the vibronic states [the red lines in Fig. 1(c)].

We also calculated the RIXS spectra of cubic K_2IrBr_6 at 270 K. For the calculation, we used the vibronic states with $g = 1.5$ and the Lorentzian function with $\Gamma = 40$ meV. We estimated g for K_2IrBr_6 from g for K_2IrCl_6 by using the relation between g and M , $g \propto M^{1/4}$. Figure 1(d) shows a good agreement between the calculated and experimental RIXS spectra [10]. The calculated spectrum has two peaks at 0.587 eV and 0.617 eV, and the gap between them (30 meV) is smaller than that of K_2IrCl_6 , which is in line with the experimental observation (the gap is 33 meV) [10].

To confirm the validity of our interaction parameters, we performed *ab initio* calculations. The calculated interaction parameters are $\lambda = 0.469$ eV, $\omega = 40.7$ meV, and $g = 0.94$ for K_2IrCl_6 and $\lambda = 0.472$ eV, $\omega = 24.5$ meV, and $g = 1.03$ for K_2IrBr_6 . The calculated λ and ω are close to the experimental values: the calculated data are about 10 % larger than the experimental data [8, 10, 12]. The g for K_2IrBr_6 is larger than that of K_2IrCl_6 , which is in line with our estimations above. The overestimation of λ and ω is due to insufficient delocalization of the t_{2g} orbitals over the ligands within the post Hartree-Fock method. Due to the overestimation of ω 's, the g 's are underestimated. Overall, we conclude that the *ab initio* calculations support the validity of the parameters extracted from the experimental data and the mechanism of the splitting.

Based on our interaction parameters, we rule out the

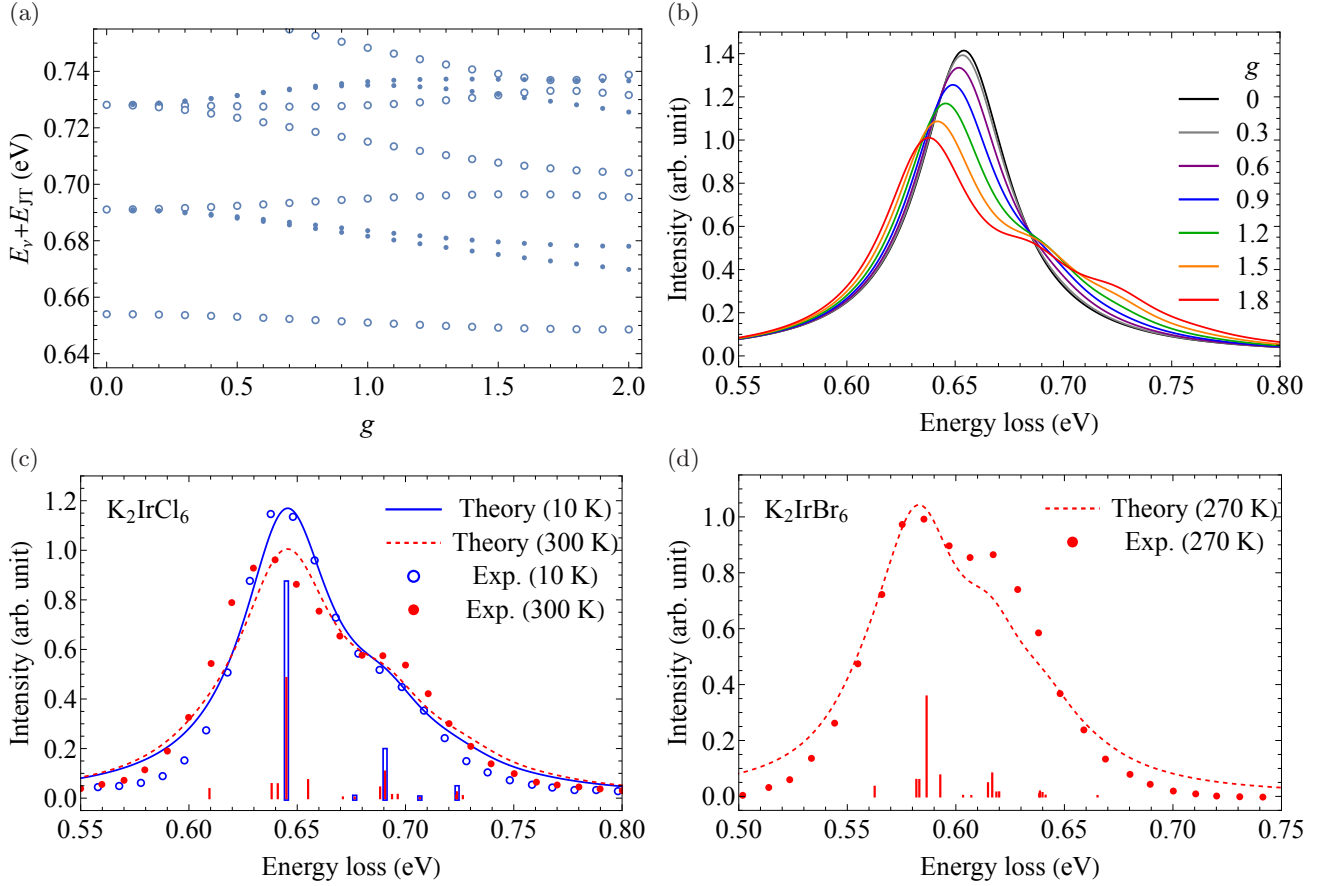


FIG. 1. Vibronic levels and RIXS spectra for (a)-(c) K_2IrCl_6 and (d) K_2IrBr_6 . (a) The vibronic spectra with respect to g . $E_{JT} = \hbar\omega(g/2)^2/2$. (b) The RIXS spectra with respect to g at $T = 10$ K. (c) Theoretical ($g = 1.2$) and the experimental [8] RIXS spectra at $T = 10$ K and $T = 300$ K. The vertical lines indicate the cross-sections ($\times 10$) at 10 K (blue) and at 300 K (red). (d) Theoretical ($g = 1.5$) and the experimental [10] RIXS spectra at $T = 270$ K.

non-cubic (or static JT effect) scenario. The JT deformations that reproduce the splitting of the $j = 3/2$ peak correspond to the shifts of the ligand atoms of about 0.007 \AA for K_2IrCl_6 and 0.004 \AA for K_2IrBr_6 . Such large shifts were not observed in the x-ray and neutron diffraction data of K_2IrCl_6 down to low temperature.

Finally, we propose that the rotational modes of the octahedra enlarge the line width of the RIXS spectra. The rotational modes quadratically couple to the t_{2g} orbitals [10] and, hence, they can contribute to the spin-orbit and lattice entanglement as the JT active modes. The rotational modes will give rise to new transitions between the levels around $j = 1/2$ and $j = 3/2$ with about one order of magnitude smaller gaps than the splitting of the $j = 3/2$ peak according to their frequencies: within the present resolution of energy, these transitions will enlarge the line width of the spectra. Due to the enlargement of the line width by raising the temperature, the peak positions of the spectra will shift, and hence, the energy gap will slightly increase.

V. CONCLUSION

In this work, we theoretically demonstrated that the dynamic JT effect determines the shape and the temperature dependence of the RIXS spectra of K_2IrCl_6 . In particular, the dynamic JT effect in the $j = 3/2$ multiplet states develops and splits the peak for the $j = 3/2$ multiplet in the RIXS spectra. The interaction parameters used for the simulations are consistent with our *ab initio* interaction parameters. Our results indicate that the system is cubic due to the dynamic JT effect. The present results suggest that the RIXS spectra of spin-orbit Mott insulators with (quasi) degenerate multiple states on sites have to be interpreted fully considering the dynamic (pseudo) JT effect.

ACKNOWLEDGMENTS

This work was partly supported by the Iketani Science and Technology Foundation and Grant-in-Aid for Scientific Research (Grant No. 22K03507) from the Japan

-
- [1] H. Takagi, T. Takayama, G. Jackeli, G. Khaliullin, and S. E. Nagler, Concept and realization of Kitaev quantum spin liquids, *Nat. Rev. Phys.* **1**, 264 (2019).
- [2] T. Takayama, J. Chaloupka, A. Smerald, G. Khaliullin, and H. Takagi, Spin-Orbit-Entangled Electronic Phases in 4d and 5d Transition-Metal Compounds, *J. Phys. Soc. Jpn.* **90**, 062001 (2021).
- [3] S. Trebst and C. Hickey, Kitaev materials, *Phys. Rep.* **950**, 1 (2022).
- [4] G. Jackeli and G. Khaliullin, Mott Insulators in the Strong Spin-Orbit Coupling Limit: From Heisenberg to a Quantum Compass and Kitaev Models, *Phys. Rev. Lett.* **102**, 017205 (2009).
- [5] I. Kimchi, J. G. Analytis, and A. Vishwanath, Three-dimensional quantum spin liquids in models of harmonic-honeycomb iridates and phase diagram in an infinite- D approximation, *Phys. Rev. B* **90**, 205126 (2014).
- [6] A. M. Cook, S. Matern, C. Hickey, A. A. Aczel, and A. Paramakanti, Spin-orbit coupled $j_{\text{eff}} = 1/2$ iridium moments on the geometrically frustrated fcc lattice, *Phys. Rev. B* **92**, 020417 (2015).
- [7] N. Khan, D. Prishchenko, Y. Skourski, V. G. Mazurenko, and A. A. Tsirlin, Cubic symmetry and magnetic frustration on the fcc spin lattice in K_2IrCl_6 , *Phys. Rev. B* **99**, 144425 (2019).
- [8] D. Reig-i Plessis, T. A. Johnson, K. Lu, Q. Chen, J. P. C. Ruff, M. H. Upton, T. J. Williams, S. Calder, H. D. Zhou, J. P. Clancy, A. A. Aczel, and G. J. MacDougall, Structural, electronic, and magnetic properties of nearly ideal $J_{\text{eff}} = \frac{1}{2}$ iridium halides, *Phys. Rev. Mater.* **4**, 124407 (2020).
- [9] L. Bhaskaran, A. N. Ponomaryov, J. Wosnitza, N. Khan, A. A. Tsirlin, M. E. Zhitomirsky, and S. A. Zvyagin, Antiferromagnetic resonance in the cubic iridium hexahalides $(\text{NH}_4)_2\text{IrCl}_6$ and K_2IrCl_6 , *Phys. Rev. B* **104**, 144404 (2021).
- [10] N. Khan, D. Prishchenko, M. H. Upton, V. G. Mazurenko, and A. A. Tsirlin, Towards cubic symmetry for Ir^{4+} : Structure and magnetism of the antiferromagnetic K_2IrBr_6 , *Phys. Rev. B* **103**, 125158 (2021).
- [11] W. Tian, Q. Chen, A. A. Aczel, C. R. Wiebe, H. Zhou, and J. Cheng, Magnetic properties of Cs_2IrCl_6 single crystals, APS March Meeting 2023, G39.3.
- [12] S. Lee, B. H. Kim, M.-J. Seong, and K.-Y. Choi, Noncubic local distortions and spin-orbit excitons in K_2IrCl_6 , *Phys. Rev. B* **105**, 184433 (2022).
- [13] H. Takahashi, H. Suzuki, J. Bertinshaw, S. Bette, C. Mühle, J. Nuss, R. Dinnebier, A. Yaresko, G. Khaliullin, H. Gretarsson, T. Takayama, H. Takagi, and B. Keimer, Nonmagnetic $J = 0$ State and Spin-Orbit Excitations in K_2RuCl_6 , *Phys. Rev. Lett.* **127**, 227201 (2021).
- [14] N. Iwahara and S. Shikano, Vibronic excitations in resonant inelastic x-ray scattering spectra of K_2RuCl_6 , *Phys. Rev. Res.* **5**, 023051 (2023).
- [15] N. Iwahara, V. Vieru, and L. F. Chibotaru, Spin-orbital-lattice entangled states in cubic d^1 double perovskites, *Phys. Rev. B* **98**, 075138 (2018).
- [16] S. Sugano, Y. Tanabe, and H. Kamimura, *Multiplets of Transition-Metal Ions in Crystals* (Academic Press, New York, 1970).
- [17] I. B. Bersuker and V. Z. Polinger, *Vibronic Interactions in Molecules and Crystals* (Springer-Verlag, Berlin and Heidelberg, 1989).
- [18] J. J. Sakurai, *Advanced Quantum Mechanics* (Addison-Wesley, Massachusetts, 1967).
- [19] L. J. P. Ament, M. van Veenendaal, T. P. Devereaux, J. P. Hill, and J. van den Brink, Resonant inelastic x-ray scattering studies of elementary excitations, *Rev. Mod. Phys.* **83**, 705 (2011).
- [20] J. Luo, G. T. Trammell, and J. P. Hannon, Scattering operator for elastic and inelastic resonant x-ray scattering, *Phys. Rev. Lett.* **71**, 287 (1993).
- [21] M. van Veenendaal, Polarization Dependence of L - and M -Edge Resonant Inelastic X-Ray Scattering in Transition-Metal Compounds, *Phys. Rev. Lett.* **96**, 117404 (2006).
- [22] N. Iwahara, V. Vieru, L. Ungur, and L. F. Chibotaru, Zeeman interaction and Jahn-Teller effect in the Γ_8 multiplet, *Phys. Rev. B* **96**, 064416 (2017).
- [23] L. Seijo and Z. Barandiarán, Computational Modelling of the Magnetic Properties of Lanthanide Compounds, in *Computational Chemistry: Reviews of Current Trends*, Vol. 4, edited by J. Leszczynski (World Scientific, Singapore, 1999) pp. 55–152.
- [24] B. O. Roos, R. Lindh, P.-Å. Malmqvist, V. Veryazov, and P.-O. Widmark, *Multiconfigurational Quantum Chemistry* (Wiley, New Jersey, 2016).
- [25] A. A. Granovsky, Extended multi-configuration quasi-degenerate perturbation theory: The new approach to multi-state multi-reference perturbation theory, *J. Chem. Phys.* **134**, 214113 (2011).
- [26] T. Shiozaki, W. Győrffy, P. Celani, and H.-J. Werner, Extended multi-state complete active space second-order perturbation theory: Energy and nuclear gradients, *J. Chem. Phys.* **135**, 081106 (2011).
- [27] I. Fdez. Galván *et al.*, OpenMolcas: From Source Code to Insight, *J. Chem. Theor. Comput.* **15**, 5925 (2019).
- [28] F. Aquilante *et al.*, Modern quantum chemistry with [Open]Molcas, *J. Chem. Phys.* **152**, 214117 (2020).